Strong-coupling expansions for the attractive Holstein and Hubbard models

J. K. Freericks
Institute for Theoretical Physics and Department of Physics, University of California, Santa Barbara, California 93106-4030
(Received 22 February 1993)

A strong-coupling expansion for the Holstein (electron-phonon) model is carried out through fourth order. In the large-frequency limit the expansion agrees with known results for the attractive Hubbard model. Mean-field theory is employed to determine transition temperatures of the effective (pseudospin) Hamiltonian and the results are compared with recent Monte Carlo simulations of these models in infinite dimensions.

I. INTRODUCTION

The interaction of conduction electrons in a solid with lattice phonons is called the electron-phonon problem. Migdal[1] and Eliashberg[2] pioneered the study of such interacting fermion-boson systems in the limit where the phonon energy scale is much smaller than the electronic energy scale. Vertex corrections can be neglected in this case[1] and a self-consistent theory can be constructed that is exact in the limit of weak coupling; the theory is an expansion in powers of the coupling strength. In the opposite limit of strong coupling, the electron pairs are strongly bound together into bipolarons and the ground state of the system is highly degenerate. Degenerate perturbation theory about this bipolaronic ground state produces a theory that is an expansion in inverse powers of the coupling strength.[3]

The simplest electron-phonon Hamiltonian is the Holstein Hamiltonian[4] in which the conduction electrons interact with local phonon modes:

$$H=-\sum_{i,j,\sigma} t_{ij}c_{i\sigma}^{\dagger}c_{j\sigma}+\sum_i (gx_i-\mu)(n_{i\uparrow}+n_{i\downarrow}) +\frac{1}{2}M\Omega^2\sum_i x_i^2+\frac{1}{2M}\sum_i p_i^2 , \tag{1}$$

where $c_{i\sigma}^{\dagger}(c_{i\sigma})$ creates (destroys) an electron at site i with spin σ, $n_{i\sigma}=c_{i\sigma}^{\dagger}c_{i\sigma}$ is the electron number operator, and $x_i(p_i)$ is the phonon coordinate (momentum) at site i. The hopping of electrons between lattice sites i and j is governed by the hopping matrix element t_{ij} (t_{ij} is a Hermitian matrix).

The local phonon has a mass M and a frequency Ω associated with it; the combination $\kappa\equiv M\Omega^2$ is a spring constant that measures the stored energy per unit length squared in the phonon coordinate. The electron-phonon interaction strength is parametrized by an energy per unit length and is denoted g. A useful combination of fundamental parameters is the bipolaron binding energy

$$U\equiv-\frac{g^2}{M\Omega^2}=-\frac{g^2}{\kappa} , \tag{2}$$

which determines the energy scale for the effective electron-electron interaction mediated by the phonon. The chemical potential is denoted by μ and the particle-hole symmetric point (half-filled band) corresponds to $\mu=U$.

The hopping matrix elements t_{ij} are used to define an energy scale. The mass is then set equal to one ($M=1$) leaving $|U|$ and Ω as free parameters. The strong-coupling expansion is a perturbative expansion in the hopping terms of Eq. (1) and is valid when the bipolaron binding energy is much larger than the electronic energy scale ($|U|\gg|t_{ij}|$). The only remaining degree of freedom in the strong-coupling regime is the polaron band narrowing parameter denoted $S=|U|/\Omega$.

In the limit where the phonon frequency becomes very large $\Omega\to\infty$ ($S\to 0$), the effective electron-electron interaction is instantaneous and the Holstein model becomes an attractive Hubbard model[5]

$$H=-\sum_{i,j,\sigma} t_{ij}c_{i\sigma}^{\dagger}c_{j\sigma}+U\sum_i\left[n_{i\uparrow}-\frac{1}{2}\right]\left[n_{i\downarrow}-\frac{1}{2}\right] +(U-\mu)\sum_i (n_{i\uparrow}+n_{i\downarrow}) , \tag{3}$$

with the electron-electron interaction strength U determined by Eq. (2).

Recent work on the Holstein Hamiltonian has found that the effective phonon potential becomes anharmonic, developing a double-well structure at small to moderate values of $|U|$.[6-9] A double-well structure signifies the formation of a bipolaron and indicates that a strong-coupling expansion should be accurate down to moderate values of $|U|$. This observation provides a motivation for studying the strong-coupling expansion to determine its region of validity.

Strong-coupling expansions have a rich history. In the late 1950's Anderson[10] showed that the strong-interaction-strength limit of the Hubbard model is described by a Heisenberg antiferromagnet with an exchange integral $j=4|t_{ij}|^2/|U|$ that vanishes as the interaction strength increases. Since then, two competing methods have been employed to determine the effective Hamiltonian in the strong-coupling limit: methods based upon perturbation theory, and methods based upon canonical transformations. Kato[11] described how to determine an effective Hamiltonian for a degenerate sub-

0163-1829/93/48(6)/3881(11)/$06.00

space using perturbation theory and standard operator methods. His analysis was applied to the Hubbard model in one dimension by Klein and Seitz[12] and in arbitrary dimensions by Takahashi.[13] Beni, Pincus, and Kanamori[14] and Hirsch and Fradkin[15] applied the same methods to the Holstein model determining the effective Hamiltonian to second order in the hopping. The canonical transformation method was motivated by the work of Lang and Firsov[16] and Schrieffer and Wolff.[17] The effective Hamiltonian for the Hubbard model was determined to lowest order by Harris and Lange[18] and carried out to very high order by MacDonald, Girvin, and Yashioka[19] using a computer algorithm.

The perturbation theory methods are applied to the Holstein Hamiltonian in Sec. II and the effective strong-coupling Hamiltonian is determined through fourth order in the hopping matrix elements. The phase diagram of the Holstein model is determined exactly in the large-dimensional limit by applying mean-field theory to the effective Hamiltonian in Sec. III, and the strong-coupling calculations are compared to exact quantum Monte Carlo simulations to determine their region of validity. Conclusions are presented in Sec. IV.

II. PERTURBATION THEORY AND THE EFFECTIVE HAMILTONIAN

In the strong-coupling limit $|U|\rightarrow\infty$, the ground state is a bipolaronic state consisting of paired electrons or zero electrons at each lattice site. Since the distribution of these paired sites is not determined from the Hamiltonian, the ground state is highly degenerate. The effective Hamiltonian (within this degenerate subspace) that determines the perturbed eigenvalues can be found by using standard operator methods.[11–13]

Consider a Hamiltonian $H=H_0+T$ with H_0 the unperturbed Hamiltonian and T the perturbation. The ground-state energy is E_0, Q_0 denotes the subspace that contains all of the degenerate ground states, and the projection operator onto Q_0 is P_0:

$$H_0P_0=P_0H_0=E_0P_0\ ,\quad P_0^2=P_0\ . \tag{4}$$

As the perturbation is turned on, the eigenstates will evolve into a new subspace Q with corresponding projection operator P. If it is assumed that the subspace Q has a nonzero overlap with the unperturbed subspace Q_0, then the standard eigenvalue equation $(H-E)|E\rangle=0$ can be projected onto the unperturbed subspace Q_0,

$$P_0(H-E)PP_0|E\rangle=0\ , \tag{5}$$

to yield an effective equation for the perturbed eigenvalue E. The Hamiltonian P_0HPP_0 acts purely within the unperturbed subspace Q_0 and has an overlap operator P_0PP_0 that is not equal to the identity. This overlap operator can be removed[20] to yield an effective Hamiltonian within the unperturbed subspace Q_0

$$H_{\rm eff}=(P_0PP_0)^{-1/2}P_0HPP_0(P_0PP_0)^{-1/2}\ , \tag{6}$$

where

$$(P_0PP_0)^{-1/2}\equiv P_0+\sum_{n=1}^{\infty}\frac{(2n-1)!!}{(2n)!!}[P_0(P_0-P)P_0]^n\ , \tag{7}$$

and

$$P=P_0-\sum_{n=1}^{\infty}\sum_{\substack{k_1+k_2+\cdots+k_{n+1}=n\\ k_i\geq 0}}R^{k_1}TR^{k_2}T\cdots TR^{k_{n+1}}\ . \tag{8}$$

The operator R^k is defined to be

$$R^0\equiv -P_0\ ,\quad R^k\equiv[(1-P_0)/(E_0-H_0)]^k\ \text{ for } k\geq 1\ . \tag{9}$$

In the case of the Holstein Hamiltonian with H_0 chosen by Eq. (1) with $t_{ij}\equiv 0$, the effective Hamiltonian is only a function of even powers of the perturbation ($H_{\rm eff}=H_0+H_2+H_4+\cdots$). The first two terms of the effective Hamiltonian satisfy

$$H_2\equiv P_0T\frac{1-P_0}{E_0-H_0}TP_0\ , \tag{10}$$

and

$$\begin{aligned}H_4\equiv{}&P_0T\frac{1-P_0}{E_0-H_0}T\frac{1-P_0}{E_0-H_0}T\frac{1-P_0}{E_0-H_0}TP_0\\&-\frac{1}{2}\left[P_0T\frac{1-P_0}{(E_0-H_0)^2}TP_0T\frac{1-P_0}{E_0-H_0}TP_0\right.\\&\left.+P_0T\frac{1-P_0}{E_0-H_0}TP_0T\frac{1-P_0}{(E_0-H_0)^2}TP_0\right]\ .\end{aligned} \tag{11}$$

The expansion for the effective Hamiltonian can be expressed graphically by a set of diagrams. A solid line denotes the hopping of an electron from site i to site j and is governed by the matrix element t_{ij}. The diagrams must be closed, since the effective Hamiltonian acts within the degenerate subspace Q_0. There is only one possibility for the second-order term, which corresponds to hopping from site i to site j and hopping back to site i, or which corresponds to subsequent hops from site i to site j. The diagram is illustrated schematically in Fig. 1(a). There are four possible diagrams that can contribute to fourth order which are depicted in Fig. 1. The first three diagrams are linked diagrams which form nonvanishing contributions to the effective Hamiltonian. The last diagram 1(e) is an unlinked diagram which does not contribute to the effective Hamiltonian because the contributions from the positive and negative terms in Eq. (11) cancel. The unlinked diagrams must cancel in order to have an energy per lattice site that is finite in the thermodynamic limit. The fourth-order terms fall into three categories, those that link two distinct sites [Fig. 1(b)], three distinct sites [Fig. 1(c)], or four distinct sites [Fig. 1(d)].

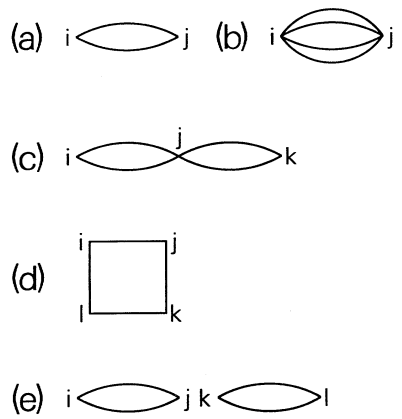

FIG. 1. Schematic diagrams used in the determination of the effective Hamiltonian. The second-order diagram is plotted in (a), while the fourth-order diagrams appear in (b)–(e). The fourth-order diagrams link two (b), three (c), or four (d) distinct lattice sites. The contributions from the unlinked diagram (e) vanish.

The matrix elements for the effective Hamiltonian are evaluated by introducing appropriate complete sets of states between each of the operator factors in Eqs. (10) and (11). The expectation value of the operator E_0-H_0 is $-\Omega(m+nS)$ where m is the total quantum number of all of the excited harmonic oscillator states and n is the total number of broken electron pairs. The limit of large frequency $\Omega\rightarrow\infty$ is simple because the intermediate state must always lie in a harmonic-oscillator ground state ($m=0$) and the expectation value of E_0-H_0 depends only upon the number of broken pairs. The limit of small frequency $\Omega\rightarrow 0$ is problematic because the unperturbed subspace Q_0 is larger for $\Omega=0$ than for nonzero Ω.

We will be interested in evaluating thermodynamic phase transitions at finite temperatures. An approximation is made that the transition temperature T_c is much smaller than the phonon frequency Ω so that one can restrict the analysis to the subspace Q_0 corresponding to the ground state and need not consider the effective Hamiltonian in the subspaces corresponding to excited states. This is not a prohibitive approximation since the small-frequency limit is already known to be singular.

The evaluation of the second-order Hamiltonian H_2 has been performed previously.[14,15] It is instructive to illustrate its calculation in the present framework since it is simpler than the calculation of the fourth-order terms.

The origin of the harmonic oscillator lies at $x_0=0$, $x_0=-g/M\Omega^2$, or $x_0=-2g/M\Omega^2$ when there are zero, one, or two electrons, respectively, at a given lattice site. Let $|+m\rangle$, $|m\rangle$, and $|-m\rangle$ denote the mth harmonic-oscillator state centered about the origin with zero, one, and two electrons, respectively. The overlaps $\langle\pm m|n\rangle$ satisfy

$$\langle\pm m|n\rangle=\frac{1}{\sqrt{m!n!}}e^{-(S/4)}\times\langle 0|(a\pm\sqrt{S/2})^m(a^\dagger\mp\sqrt{S/2})^n|0\rangle\ , \tag{12}$$

where $a^\dagger$ (a) is the harmonic-oscillator creation (annihilation) operator.

When site i is occupied by an electron pair and site j is unoccupied, the electron pair separates with one electron hopping from site i to site j and either hopping back from site j to site i or the second electron hopping from site i to site j. There is only one class of intermediate states

$$\uparrow\downarrow\ 0\Longrightarrow\uparrow\ \downarrow\Longrightarrow\uparrow\downarrow\ 0\ , \tag{13}$$

$$\uparrow\downarrow\ 0\Longrightarrow\uparrow\ \downarrow\Longrightarrow\ 0\ \uparrow\downarrow\ , \tag{14}$$

where $\uparrow\downarrow$ corresponds to a bipolaron on a lattice site, 0 corresponds to an empty lattice site, and $\uparrow$ or $\downarrow$ corresponds to a single electron (polaron) at a lattice site. Only one of the two possible intermediate states is shown in Eqs. (13) and (14). Consider first the evaluation of Eq. (13). Introducing the relevant complete sets of states produces

$$\Delta(i,j)\equiv\sum_{m,n=0}^{\infty}2t_{ij}^2\frac{\langle-0|m\rangle\langle+0|n\rangle\langle m|-0\rangle\langle n|+0\rangle}{-\Omega(m+n+S)}=-\frac{2t_{ij}^2}{|U|}Se^{-S}\sum_{m,n=0}^{\infty}\frac{S^{m+n}}{m!n!}\frac{1}{m+n+S}\ , \tag{15}$$

for the diagonal matrix elements of the effective Hamiltonian. Similarly one finds

$$\Delta'(i,j)\equiv\sum_{m,n=0}^{\infty}2t_{ij}^2\frac{\langle-0|m\rangle\langle+0|n\rangle\langle m|+0\rangle\langle n|-0\rangle}{-\Omega(m+n+S)}=-\frac{2t_{ij}^2}{|U|}Se^{-S}\sum_{m,n=0}^{\infty}\frac{(-S)^{m+n}}{m!n!}\frac{1}{m+n+S}\ , \tag{16}$$

for the evaluation of Eq. (14). Using the identity

$$\sum_{m,n=0}^{\infty}\frac{x^{m+n}}{m!n!}\frac{1}{m+n+y}=\frac{1}{y}e^{2x}\left[1+\sum_{n=1}^{\infty}\frac{(-2x)^n}{(y+1)(y+2)\cdots(y+n)}\right]\ , \tag{17}$$

yields the simplification

$$\Delta(i,j)=-\frac{2t_{ij}^2}{|U|}\left[1+\sum_{n=1}^{\infty}\frac{(-S)^n}{(S+1)(S+2)\cdots(S+n)}\right]\ , \tag{18}$$

$$\Delta'(i,j)=-\frac{2t_{ij}^2}{|U|}e^{-2S}\times\left[1+\sum_{n=1}^{\infty}\frac{S^n}{(S+1)(S+2)\cdots(S+n)}\right]\ .$$

At this point, it is convenient to introduce the notion of pseudospin operators.[21] If the lattice is bipartite,[22] so that it can be separated into A and B sublattices with nonzero hopping matrix elements only between sublattices A and B, then one can define pseudospin operators via

$$J_j^+=(-1)^j c_{j\uparrow}^\dagger c_{j\downarrow}^\dagger\ ,\quad J_j^-=(J_j^+)^\dagger\ ,\quad J_j^z=\tfrac{1}{2}(n_{j\uparrow}+n_{j\downarrow}-1)\ , \tag{19}$$

and the factor $(-1)^j$ is 1 for the A sublattice and (-1) for the B sublattice. The pseudospin operators satisfy an SU(2) algebra and form a spin-$\frac{1}{2}$ representation in the strong-coupling limit. A doubly occupied site corresponds to an up pseudospin and an empty site corresponds to a down pseudospin. The matrix elements of the effective Hamiltonian (that connects site i to site j) satisfy

$$H_2(i,j)|\uparrow\uparrow\rangle=0\ ,$$
$$H_2(i,j)|\uparrow\downarrow\rangle=\Delta(i,j)|\uparrow\downarrow\rangle-\Delta'(i,j)|\downarrow\uparrow\rangle\ , \tag{20}$$

with similar results for the pseudo-spin-flipped states. So the effective Hamiltonian can be mapped onto a pseudospin Hamiltonian (with the same matrix elements) that corresponds to an XXZ Heisenberg antiferromagnet

$$H_2=\tfrac{1}{2}\sum_{i,j}\left[j_\perp^{(2)}(i,j)\frac{1}{2}(J_i^+J_j^-+J_i^-J_j^+)+j_\parallel^{(2)}(i,j)\left[J_i^zJ_j^z-\frac{1}{4}\right]\right]\ , \tag{21}$$

with

$$j_\perp^{(2)}(i,j)\equiv-2\Delta'(i,j)$$

and

$$j_\parallel^{(2)}(i,j)\equiv-2\Delta(i,j)\ .$$

Note that the summation in Eq. (21) is not restricted to $i<j$.

The fourth-order terms can be separated into three distinct forms $H_4=H_4(b)+H_4(c)+H_4(d)$ corresponding to each of the linked fourth-order diagrams in Fig. 1. The fourth-order term $H_4(b)$ corresponding to Fig. 1(b) may be determined in a similar fashion to the second-order term. The effective Hamiltonian is identical in form to Eq. (21) with exchange integrals $j_\perp^{(4)}(i,j)$ and $j_\parallel^{(4)}(i,j)$. The intermediate states needed for the calculation of the parallel exchange parameter are

$$\uparrow\downarrow\ 0\Longrightarrow\uparrow\ \downarrow\Longrightarrow\uparrow\downarrow\ 0\Longrightarrow\uparrow\ \downarrow\Longrightarrow\uparrow\downarrow\ 0\ , \tag{22}$$

and

$$\uparrow\downarrow\ 0\Longrightarrow\uparrow\ \downarrow\Longrightarrow\ 0\ \uparrow\downarrow\Longrightarrow\uparrow\ \downarrow\Longrightarrow\uparrow\downarrow\ 0\ , \tag{23}$$

with a pseudospin multiplicity of four. The exchange integral becomes

$$j_\parallel^{(4)}=\frac{8t_{ij}^4}{\Omega^3}\left[\sum_{\substack{l,l',m,m',n,n'=0\\ m+m'\neq0}}^{\infty}\left[\frac{\langle+0|n\rangle\langle-0|n'\rangle\langle n|+m\rangle\langle n'|-m'\rangle\langle+m|l\rangle\langle-m'|l'\rangle\langle l|+0\rangle\langle l'|-0\rangle}{(n+n'+S)(m+m')(l+l'+S)}+\frac{\langle+0|n\rangle\langle-0|n'\rangle\langle n|-m\rangle\langle n'|+m'\rangle\langle-m|l\rangle\langle+m'|l'\rangle\langle l|+0\rangle\langle l'|-0\rangle}{(n+n'+S)(m+m')(l+l'+S)}\right]\right.$$
$$\left.-\sum_{l,l',n,n'=0}^{\infty}\left[\frac{\langle+0|n\rangle\langle-0|n'\rangle\langle n|+0\rangle\langle n'|-0\rangle\langle+0|l\rangle\langle-0|l'\rangle\langle l|+0\rangle\langle l'|-0\rangle}{(n+n'+S)^2(l+l'+S)}+\frac{\langle+0|n\rangle\langle-0|n'\rangle\langle n|-0\rangle\langle n'|+0\rangle\langle-0|l\rangle\langle+0|l'\rangle\langle l|+0\rangle\langle l'|-0\rangle}{(n+n'+S)^2(l+l'+S)}\right]\right]. \tag{24}$$

Substituting in the matrix elements from Eq. (12) and using the identities

$$\sum_{n=0}^{\infty}\frac{x^n}{n!}\frac{1}{n+y}=\int_0^1 z^{y-1}e^{xz}dz\ ,\quad \sum_{n=0}^{\infty}\frac{x^n}{n!}\frac{1}{(n+y)^2}=-\int_0^1 z^{y-1}e^{xz}\ln z\,dz\ , \tag{25}$$

and

$$\langle0|e^{ax}(a^\dagger+y)^m|0\rangle=(x+y)^m\ , \tag{26}$$

produces the final result

$$j_\parallel^{(4)}=\frac{8t_{ij}^4}{|U|^3}S^3e^{-2S}\left[\sum_{\substack{m,m'=0\\ m+m'\neq0}}\int_0^1dx\int_0^1dy(xy)^{S-1}\left[e^{S(x+y)}\frac{(S/2)^{m+m'}(1-x)^{2m}(1-y)^{2m'}}{m!m'!(m+m')}+e^{-S(x+y)}\frac{(S/2)^{m+m'}(1+x)^{2m}(1+y)^{2m'}}{m!m'!(m+m')}\right]\right.$$
$$\left.-\sum_{m,m'=0}^{\infty}\frac{S^{m+m'}}{m!m'!}\frac{1+(-1)^{m+m'}}{(m+S)^2(m'+S)}\right]. \tag{27}$$

A similar analysis for the perpendicular exchange integral gives

$$j_\perp^{(4)}=\frac{8t_{ij}^4}{|U|^3}S^3e^{-2S}\left[\sum_{\substack{m,m'=0\\ m+m'\neq 0}}^{\infty}\int_0^1dx\int_0^1dy(xy)^{S-1}2\cosh[S(x-y)]\frac{(S/2)^{m+m'}(1-x^2)^m(1-y^2)^{m'}}{m!m'!(m+m')}\right.$$
$$\left.-\sum_{m,m'=0}^{\infty}\frac{S^{m+m'}}{m!m'!}\frac{(-1)^m+(-1)^{m'}}{(m+S)^2(m'+S)}\right], \tag{28}$$

and the effective Hamiltonian becomes

$$H_4(b)=\frac{1}{2}\sum_{i,j}\left[j_\perp^{(4)}\frac{1}{2}(J_i^+J_j^-+J_i^-J_j^+)+j_\parallel^{(4)}\left[J_i^zJ_j^z-\frac{1}{4}\right]\right], \tag{29}$$

where the i,j dependence of the exchange integrals has been suppressed.

The contributions to the effective Hamiltonian $H_4(c)$ from the diagram in Fig. 1(c) can be determined by employing the same techniques. By symmetry, the most general effective Hamiltonian satisfies

$$H_4(i,j,k)|\uparrow\uparrow\uparrow\rangle=0,$$
$$H_4(i,j,k)|\uparrow\downarrow\uparrow\rangle=j_\parallel'|\uparrow\downarrow\uparrow\rangle-\frac{1}{2}j_\perp'(|\uparrow\uparrow\downarrow\rangle+|\downarrow\uparrow\uparrow\rangle),$$
$$H_4(i,j,k)|\uparrow\uparrow\downarrow\rangle=-\tfrac{1}{2}j_\parallel''|\uparrow\uparrow\downarrow\rangle-\frac{1}{2}j_\perp'|\uparrow\downarrow\uparrow\rangle+\frac{1}{2}j_\perp''|\downarrow\uparrow\uparrow\rangle, \tag{30}$$
$$H_4(i,j,k)|\downarrow\uparrow\uparrow\rangle=-\tfrac{1}{2}j_\parallel''|\downarrow\uparrow\uparrow\rangle-\frac{1}{2}j_\perp'|\uparrow\downarrow\uparrow\rangle+\frac{1}{2}j_\perp''|\uparrow\uparrow\downarrow\rangle,$$

with similar results for the pseudo-spin-flipped states (the i,j,k dependence of the coefficients is suppressed). In terms of the pseudospin operators, the contribution to the effective Hamiltonian becomes

$$H_4(c)=\frac{1}{2}{\sum_{i,j,k}}'\left[j_\perp'\frac{1}{2}(J_i^+J_j^-+J_i^-J_j^++J_k^+J_j^-+J_k^-J_j^+)-j_\parallel'\left[J_i^zJ_j^z+J_k^zJ_j^z-\frac{1}{2}\right]+j_\perp''\frac{1}{2}(J_i^+J_k^-+J_i^-J_k^+)\right.$$
$$\left.+(j_\parallel'+j_\parallel'')\left[J_i^zJ_k^z-\frac{1}{4}\right]\right], \tag{31}$$

where the prime indicates that i,j, and k are all distinct. The algebra needed to determine the effective exchange integrals is straightforward but tedious. The results are

$$j_\perp'=\frac{4t_{ij}^2t_{jk}^2}{|U|^3}S^3e^{-2S}\left[\int_0^1dx\int_0^1dy\int_0^1dz(xyz)^{S-1}\right.$$
$$\times(\exp\{\tfrac{1}{2}S[x-y+z-2z(x-y)-xyz]\}+\exp\{\tfrac{1}{2}S[x-y-z(x+y)]\})$$
$$+2\int_0^1dx\int_0^1dy(xy)^{S-1}e^{S(x-y)}\sum_{m=1}^{\infty}\frac{(S/2)^m(1-x)^m(1+y)^m}{m!m}$$
$$\left.+\int_0^1dx\int_0^1dy(xy)^{S-1}e^{S(x-y)}(\ln x+\ln y)\right], \tag{32}$$

$$j_\perp''=-\frac{4t_{ij}^2t_{jk}^2}{|U|^3}S^3e^{-2S}\left[\int_0^1dx\int_0^1dy\int_0^1dz(xyz)^{S-1}\exp\{\tfrac{1}{2}S[x+y+z-2z(x+y)+xyz]\}\right.$$
$$+2\int_0^1dx\int_0^1dy(xy)^{S-1}e^{-S(x+y)}\sum_{m=1}^{\infty}\frac{(S/2)^m(1+x)^m(1+y)^m}{m!m}$$
$$\left.+2\int_0^1dx\int_0^1dy(xy)^{S-1}e^{-S(x+y)}\ln x\right], \tag{33}$$

$$j'_{\parallel}=-\frac{4t_{ij}^2t_{jk}^2}{|U|^3}S^3e^{-2S}\left[\int_0^1dx\int_0^1dy\int_0^1dz(xyz)^{S-1}(\exp\{\tfrac{1}{2}S[-x-y+z+2z(x+y)+xyz]\}\right.$$
$$+\exp\{\tfrac{1}{2}S[-x-y+2z+z(x+y)+2xyz]\})$$
$$+2\int_0^1dx\int_0^1dy(xy)^{S-1}e^{S(x+y)}\sum_{m=1}^{\infty}\frac{(S/2)^m(1-x)^m(1-y)^m}{m!m}$$
$$\left.+2\int_0^1dx\int_0^1dy(xy)^{S-1}e^{S(x+y)}\ln x\right], \tag{34}$$

$$j''_{\parallel}=\frac{4t_{ij}^2t_{jk}^2}{|U|^3}S^3e^{-2S}\int_0^1dx\int_0^1dy\int_0^1dz(xyz)^{S-1}\exp\{\tfrac{1}{2}S[x+y+2z-z(x+y)+2xyz]\}\ . \tag{35}$$

Finally, the effective Hamiltonian $H_4(d)$ corresponding to Fig. 1(d) is evaluated. The most general pseudospin Hamiltonian for this linked diagram is

$$\begin{aligned}
&H_4(i,j,k,l)|\uparrow\uparrow\uparrow\uparrow\rangle=0\ ,\\
&H_4(i,j,k,l)|\uparrow\uparrow\uparrow\downarrow\rangle=\alpha|\uparrow\uparrow\uparrow\downarrow\rangle-\beta[|\uparrow\uparrow\downarrow\uparrow\rangle+|\downarrow\uparrow\uparrow\uparrow\rangle]+\gamma|\uparrow\downarrow\uparrow\uparrow\rangle\ ,\\
&H_4(i,j,k,l)|\uparrow\uparrow\downarrow\downarrow\rangle=\delta|\uparrow\uparrow\downarrow\downarrow\rangle-\epsilon[|\uparrow\downarrow\uparrow\downarrow\rangle+|\downarrow\uparrow\downarrow\uparrow\rangle]+\mu[|\downarrow\uparrow\uparrow\downarrow\rangle+|\uparrow\downarrow\downarrow\uparrow\rangle]\ ,\\
&H_4(i,j,k,l)|\uparrow\downarrow\uparrow\downarrow\rangle=\nu|\uparrow\downarrow\uparrow\downarrow\rangle-\epsilon[|\uparrow\uparrow\downarrow\downarrow\rangle+|\uparrow\downarrow\downarrow\uparrow\rangle+|\downarrow\uparrow\uparrow\downarrow\rangle+|\downarrow\downarrow\uparrow\uparrow\rangle]+\rho|\downarrow\uparrow\downarrow\uparrow\rangle\ ,
\end{aligned} \tag{36}$$

with similar results for both cyclically permutated and pseudo-spin-flipped states. This effective Hamiltonian can be expressed as

$$H_4(d)=\frac{1}{8}{\sum_{i,j,k,l}}'\left[\frac{\alpha}{2}+\frac{\delta}{4}+\frac{\nu}{8}-\frac{\nu}{2}(J_i^zJ_j^z+J_i^zJ_l^z+J_k^zJ_j^z+J_k^zJ_l^z)\right.$$
$$+\frac{\beta+\epsilon}{2}(J_i^+J_j^-+J_i^-J_j^++J_i^+J_l^-+J_i^-J_l^++J_k^+J_j^-+J_k^-J_j^++J_k^+J_l^-+J_k^-J_l^+)$$
$$-\left[\delta-\frac{\nu}{2}\right](J_i^zJ_k^z+J_j^zJ_l^z)+\frac{\gamma+\mu}{2}(J_i^+J_k^-+J_i^-J_k^++J_j^+J_l^-+J_j^-J_l^+)$$
$$+2(\beta-\epsilon)[J_i^zJ_j^z(J_k^+J_l^-+J_k^-J_l^+)+J_k^zJ_l^z(J_i^+J_j^-+J_i^-J_j^+)$$
$$+J_i^zJ_l^z(J_k^+J_j^-+J_k^-J_j^+)+J_k^zJ_j^z(J_i^+J_l^-+J_i^-J_l^+)]$$
$$+2(\gamma-\mu)[J_i^zJ_k^z(J_j^+J_l^-+J_j^-J_l^+)+J_j^zJ_l^z(J_i^+J_k^-+J_i^-J_k^+)]$$
$$+\frac{\rho}{2}[(J_i^+J_j^-+J_i^-J_j^+)(J_k^+J_l^-+J_k^-J_l^+)+(J_i^+J_l^-+J_i^-J_l^+)(J_k^+J_j^-+J_k^-J_j^+)$$
$$\left.-(J_i^+J_k^-+J_i^-J_k^+)(J_j^+J_l^-+J_j^-J_l^+)]+(-8\alpha+4\delta+2\nu)J_i^zJ_j^zJ_k^zJ_l^z\right], \tag{37}$$

in terms of the pseudospin operators (the i,j,k,l dependence of the coefficients has been suppressed) with the prime indicating that all four sites are distinct. The coefficients in Eq. (37) can be expressed in terms of three-dimensional integrals as

$$C=\frac{4t_{ij}t_{jk}t_{kl}t_{li}}{|U|^3}S^3e^{-2S}\int_0^1dx\int_0^1dy\int_0^1dz(xyz)^{S-1}C(x,y,z)\ , \tag{38}$$

where $C(x,y,z)$ is the integrand corresponding to the coefficient C. The integrands for the eight coefficients in Eq. (37) are recorded in Table I.

The effective pseudospin Hamiltonian $H_{\rm eff}=H_0+H_2+H_4(b)+H_4(c)+H_4(d)$ is an anisotropic, frustrated, antiferromagnetic Heisenberg model with additional quartic spin-spin interactions. In the instantaneous limit ($\Omega\rightarrow\infty$), the effective Hamiltonian becomes isotropic. In the static limit ($\Omega\rightarrow 0$), the Hamiltonian involves only the z component of the pseudospin.

An important check of the effective Hamiltonian arises from taking the instantaneous limit of $S\rightarrow 0$ which should produce the effective Hamiltonian of the Hubbard model.[13,19] In the Hubbard-model limit the parameters of the effective Hamiltonian satisfy

TABLE I. Integrands for the eight coefficients of the effective Hamiltonian $H_4(d)$.

Coefficient	Integrand for Eq. (38)
α	$-\exp\frac{1}{2}S(x+y+z+xyz)$
β	$\exp\frac{1}{2}S(-x+y+z-xyz)+\exp\frac{1}{2}S[-x+y+z(x-y)]$
γ	$-2\cosh\frac{1}{2}S[x+y-z(x+y)]-\exp\frac{1}{2}S(-x-y+z+xyz)$
δ	$2\exp\frac{1}{2}S[x+y+z(x+y)]$
ϵ	$-\exp\frac{1}{2}S(-x+y-z+xyz)-\exp\frac{1}{2}S[-x+y-z(x-y)]$ $-z^S\exp\frac{1}{2}S[2z(-x+y)]-z^S\exp\frac{1}{2}S[z+z(x-y)-xyz]$
μ	$\exp\frac{1}{2}S(x+y-z-xyz)+2z^S\cosh\frac{1}{2}S[z-z(x+y)+xyz]$
ν	$4z^S\exp\frac{1}{2}S[z+z(x+y)+xyz]$
ρ	$4\exp\frac{1}{2}S[-x-y-z(x+y)]+4\exp\frac{1}{2}S(-x-y-z-xyz)$ $+2z^S\exp\frac{1}{2}S[-2z(x+y)]+2z^S\exp\frac{1}{2}S(-z-xyz)$

$$j_\perp^{(2)}=j_\parallel^{(2)}=\frac{4t_{ij}^2}{|U|}\ ,\quad j_\perp^{(4)}=j_\parallel^{(4)}=-\frac{16t_{ij}^4}{|U|^3}\ ,\quad j_\perp'=j_\parallel'=0\ ,\quad j_\perp''=j_\parallel''=\frac{4t_{ij}^2t_{jk}^2}{|U|^3}\ ,$$
$$\alpha=-\frac{\beta}{2}=\frac{\gamma}{3}=-\frac{\delta}{2}=\frac{\epsilon}{3}=-\frac{\mu}{2}=-\frac{\nu}{2}=-\frac{\rho}{10}=-\frac{4t_{ij}t_{jk}t_{kl}t_{li}}{|U|^3}\ , \tag{39}$$

producing

$$H_{\rm eff}^{\rm Hub}=U\sum_i\left[2(J_i^z)^2-\frac{1}{4}\right]+2(U-\mu)\sum_i J_i^z+\frac{1}{2}M\Omega^2\sum_i\left[x_i+\frac{g}{M\Omega^2}(2J_i^z+1)\right]^2+\frac{1}{2M}\sum_i p_i^2$$
$$+\frac{1}{2}\sum_{i,j}\left[\frac{4t_{ij}^2}{|U|}-\frac{16t_{ij}^4}{|U|^3}\right]\left[\mathbf{J}_i\cdot\mathbf{J}_j-\frac{1}{4}\right]+\frac{1}{2}{\sum_{i,j,k}}'\frac{4t_{ij}^2t_{jk}^2}{|U|^3}\left[\mathbf{J}_i\cdot\mathbf{J}_k-\frac{1}{4}\right]$$
$$+{\sum_{i,j,k,l}}'\frac{t_{ij}t_{jk}t_{kl}t_{li}}{8|U|^3}\Big[1-4(\mathbf{J}_i\cdot\mathbf{J}_j+\mathbf{J}_i\cdot\mathbf{J}_l+\mathbf{J}_i\cdot\mathbf{J}_k+\mathbf{J}_k\cdot\mathbf{J}_j+\mathbf{J}_k\cdot\mathbf{J}_l+\mathbf{J}_j\cdot\mathbf{J}_l)$$
$$+80(\mathbf{J}_i\cdot\mathbf{J}_j\mathbf{J}_k\cdot\mathbf{J}_l+\mathbf{J}_i\cdot\mathbf{J}_l\mathbf{J}_k\cdot\mathbf{J}_j-\mathbf{J}_i\cdot\mathbf{J}_k\mathbf{J}_j\cdot\mathbf{J}_l)\Big]\ , \tag{40}$$

in agreement with the known results.[13,19]

III. MEAN-FIELD THEORY

Consider the simplified case of nearest-neighbor hopping on a hypercubic lattice in d dimensions. The hopping matrix elements satisfy

$$t_{ij}=t^*/2\sqrt{d}\ , \tag{41}$$

where i and j are nearest neighbors and are zero otherwise. The hopping matrix elements scale as the inverse square root of the dimensionality because this is the only scaling that will yield a finite kinetic energy in the limit of infinite dimensions.[23] The rescaled hopping integral t^* is chosen to be the energy unit.

Since the effective Hamiltonian

$$H_{\rm eff}=H_0+H_2+H_4(b)+H_4(c)+H_4(d)$$

is a pseudospin Hamiltonian, mean-field theory for the spin-$\frac{1}{2}$ degree of freedom can be used to approximate the thermodynamic phase transitions that correspond to staggered order along the z axis [charge-density-wave formation at the antiferromagnetic $(\pi,\pi,\ldots)$ point] or to staggered order along the x axis (superconducting order in the zero-momentum pair-field state). The mean-field theory becomes exact in the limit of infinite dimensions.

The mean-field theory is constructed by determining the molecular field at each lattice site and equating the expectation value of the magnetization with that of a free spin in an external magnetic field equal to the molecular field, $\mathbf{h}_{\rm mol}$, yielding

$$\langle\mathbf{J}\rangle=\frac{\mathbf{h}_{\rm mol}}{|\mathbf{h}_{\rm mol}|}\frac{1}{2}\tanh\frac{1}{2}\beta|\mathbf{h}_{\rm mol}|\ , \tag{42}$$

as first described by Gorter.[24] The hypercubic lattice divides into two sublattices A and B where the hopping of an electron only occurs from sublattice A to sublattice B or vice versa. The paramagnetic (or high-temperature) phase corresponds to the case of a uniform magnetization on each sublattice:

$$\langle\mathbf{J}_A\rangle=\langle\mathbf{J}_B\rangle\equiv\tfrac{1}{2}m\mathbf{e}_z=\tfrac{1}{2}(\rho_e-1)\mathbf{e}_z\ , \tag{43}$$

where $\mathbf{e}_z$ is the unit vector along the z axis and ρ_e is the electron concentration. The self-consistent equation for the magnetization becomes

$$m=\tanh\tfrac{1}{2}\beta\{2(\mu-U)+md[-j_{\parallel}^{(2)}-j_{\parallel}^{(4)}+(2d-1)(j_{\parallel}'-j_{\parallel}'')+(d-1)(\delta+\tfrac{1}{2}\nu)]+m^3d(d-1)(2\alpha-\delta-\tfrac{1}{2}\nu)\}\ . \tag{44}$$

The dependence of the chemical potential μ upon the electron concentration ρ_e can easily be determined by inverting Eq. (44).

First consider the simplified case of the Hubbard model where the effective Hamiltonian is given by (40). The transition temperature to the commensurate charge-density-wave phase occurs at a temperature where the magnetization satisfies

$$\langle \mathbf{J}_A\rangle=\tfrac{1}{2}(m+m')\mathbf{e}_z\ ,\quad \langle \mathbf{J}_B\rangle\equiv\tfrac{1}{2}(m-m')\mathbf{e}_z\ , \tag{45}$$

in the limit $m'\to 0$. The transition temperature is

$$T_c=\frac{1}{2}\rho_e(2-\rho_e)\frac{t^{*2}}{|U|}\left[1-\frac{t^{*2}}{2U^2}\left[1+\frac{1}{2}\rho_e(2-\rho_e)+\frac{1}{2d}[3-\rho_e(2-\rho_e)]\right]\right]\ , \tag{46}$$

which agrees with Takahashi's results[13] in $d=3$ [Eq. (44) was used to replace the chemical potential μ by the electron concentration $\rho_e=1+m$]. At half-filling and in the limit of infinite dimensions, the transition temperature becomes

$$T_c=t^{*2}(1-0.75t^{*2}/U^2)/|U|\ .$$

The second- and fourth-order approximations are compared to the exact Monte Carlo simulations[25–28] in Fig. 2. The second-order approximation (solid line) increases without bound as $|U|\to 0$, the fourth-order approximation (dashed line) has the correct qualitative behavior of developing a peak, but does not describe the weak-coupling region properly since $T_c=0$ for $|U|<\sqrt{3}/2$. The quantum Monte Carlo results in infinite dimensions[25–27] are represented by solid dots[29] in Fig. 2. The quantum Monte Carlo transition temperatures for three dimensions[28] are plotted with open circles in Fig. 2. The density of states at half-filling for a hypercubic lattice in infinite dimensions is $0.564/t^*$ and in three dimensions is $0.494/t^*$, implying that the charge-density-wave transition temperature should be smaller in three dimensions than it is in infinite dimensions in the weak-coupling regime [it appears that the Monte Carlo results in three dimensions overestimate I_c (see Fig. 2)]. Furthermore, in the strong-coupling limit the transition temperature will *decrease* as a function of dimensionality. This arises from two sources: first the $1/d$ corrections to the negative coefficient of the $t^{*4}/|U|^3$ term increase its magnitude, decreasing T_c; second the corrections due to quantum fluctuations will reduce the transition temperature below that predicted by the mean-field theory. The quantum Monte Carlo results for infinite dimensions therefore form an *upper bound* to the transition temperature in finite dimensions in the strong-coupling regime ($|U|\geq 5$).

The transition temperature to the charge-density-wave (CDW) state for the Holstein model in the infinite-dimensional limit satisfies

$$T_c=\tfrac{1}{2}\rho_e(2-\rho_e)(dj_{\parallel}^{(2)}-d^2\{6j_{\parallel}'+2j_{\parallel}''+2(\rho_e-1)^2\alpha-\rho_e(2-\rho_e)\delta+[1+\tfrac{1}{2}\rho_e(2-\rho_e)]\nu\})\ . \tag{47}$$

The numerical evaluation of the coefficients in Eq. (47) is described in the Appendix. The second-order approximation (solid line) and fourth-order approximation (dashed line) are compared to the quantum Monte Carlo results of Ref. 9 at $\Omega=0.5$ in Fig. 3. One can see that the strong-coupling approximation is much more accurate for the Holstein model (with a moderate value of Ω) than for the Hubbard model. Once again the fourth-order approximation has the correct qualitative behavior of developing a peak but vanishes for values of $|U|$ less than 0.76. Here the peak position and magnitude are predicted quite accurately by the strong-coupling approximation.

The superconducting (SC) transition temperature is determined by finding the temperature where the magnetization satisfies

$$\langle J_A^z\rangle=\langle J_B^z\rangle=\tfrac{1}{2}m\ ,\quad \langle J_A^x\rangle=-\langle J_B^x\rangle=\tfrac{1}{2}m'\ , \tag{48}$$

in the limit $m'\to 0$. The transition temperature in the infinite-dimensional limit is

$$T_c=\frac{\rho_e-1}{\ln[\rho_e/(2-\rho_e)]}\times\{dj_{\perp}^{(2)}+d^2[4j_{\perp}'-2j_{\perp}''+2\beta-\gamma+2\epsilon-\mu+(\rho_e-1)^2(2\beta-\gamma-2\epsilon+\mu)]\}\ , \tag{49}$$

and the numerical evaluation of the parameters in Eq. (49) is discussed in the appendix. In the limit $\Omega\to\infty$, the superconducting transition temperature is always larger than the CDW transition temperature, becoming equal at half-filling ($\rho_e=1$). For finite Ω, the system is superconducting when $|U|\ll\Omega$ and has CDW order when $|U|\gg\Omega$. The phase diagram for the transition between SC and CDW order is determined by equating the transition temperatures in Eqs. (47) and (49) and determining the critical electron concentration ρ_e as a function of S and $|U|$. The result is plotted in Fig. 4 for the case $\Omega=0.5$. The second-order approximation is represented with a solid line, the fourth-order approximation with a

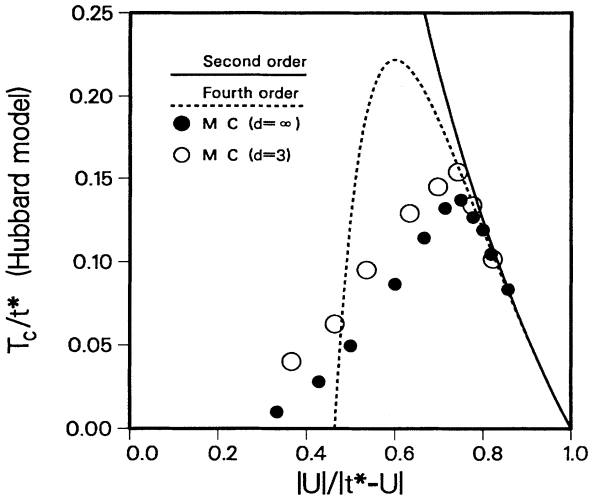

FIG. 2. Comparison of the second-order (solid line) and fourth-order (dashed line) strong-coupling approximations with the quantum Monte Carlo results (Refs. 25–27) (solid dots) for the charge-density-wave transition temperature at half-filling in the infinite-dimensional Hubbard model. The open circles are the three-dimensional quantum Monte Carlo results of Ref. 28.

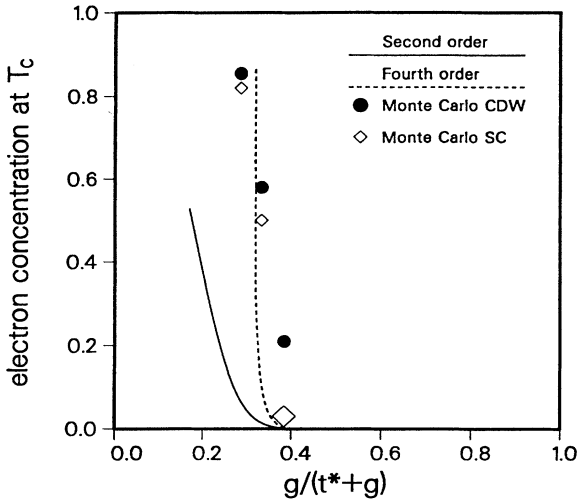

FIG. 4. Phase diagram for the transition from charge-density-wave order to superconducting order in the infinite-dimensional Holstein model with $\Omega=0.5$. The second-order approximation (solid line) and the fourth-order approximation (dashed line) are compared to the quantum Monte Carlo results (Ref. 9). The Monte Carlo simulations predict that the transition occurs between the last observed charge-density-wave transition (solid dot) and the first superconducting transition (open diamond).

dashed line, and the quantum Monte Carlo results[9] with a solid dot for a CDW transition and an open diamond for a SC transition. One can see that the fourth-order approximation is superior to the second-order approximation, but neither describes the transition region well.

To understand the origin of why the strong-coupling approximation predicts the CDW transition temperature at half-filling so accurately, but fails to predict the CDW-SC transition as well, the CDW transition temperature at $g=0.625$ ($|U|=1.5625$), $\Omega=0.5$ is plotted as a function of electron concentration in Fig. 5. The fourth-order result overestimates T_c by approximately 2–5 % at half-filling and the quantum Monte Carlo overestimates T_c by a similar amount (5%) for all fillings because of a systematic Trotter error (the quantum Monte Carlo results were calculated at $\Delta\tau=0.4$ and were not scaled to

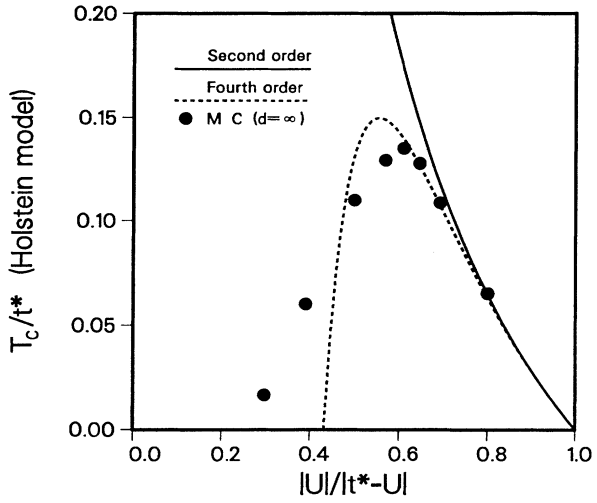

FIG. 3. Comparison of the second-order (solid line) and fourth-order (dashed line) strong-coupling approximations with the quantum Monte Carlo results (Ref. 9) (solid dots) for the charge-density-wave transition temperature at half-filling in the infinite-dimensional Holstein model with $\Omega=0.5$.

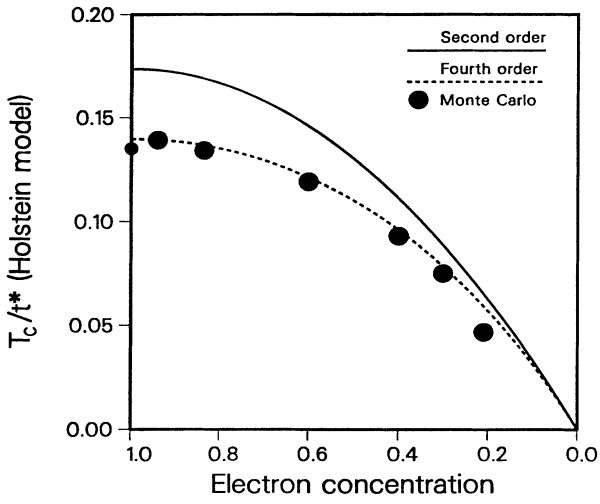

FIG. 5. Charge-density-wave transition temperature vs electron concentration for the infinite-dimensional Holstein model at $g=0.625$ ($|U|=1.5625$) and $\Omega=0.5$. The second-order approximation (solid line) is compared with the fourth-order approximation (dashed line) and the quantum Monte Carlo results (Ref. 9) (solid dots).

reduce the Trotter error[9]). Note that the agreement is poorest at the lowest electron concentration indicating that the error in the strong-coupling approximation grows as the electron concentration is reduced. As a result, the strong-coupling approximation fails to accurately predict the CDW-SC transition because it severely overestimates the CDW transition temperature at low electron concentrations.

IV. CONCLUSIONS

The strong-coupling expansion has been evaluated through fourth order in the hopping for the Holstein model. The result is an anisotropic, frustrated, antiferromagnetic Heisenberg Hamiltonian with quartic spin-spin interactions. The instantaneous limit ($\Omega\rightarrow\infty$) produces the known results[12,13,19] for the Hubbard model. The approximation was compared to recent quantum Monte Carlo simulations for the Hubbard[25–27] and Holstein[9] models and found to agree quite well in the strong-coupling regime. Agreement was significantly better for the Holstein model at $\Omega=0.5$ than for the Hubbard model.

The second-order strong-coupling approximation predicts transition temperatures that diverge as the interaction strength vanishes. The fourth-order approximation, however, has the correct qualitative behavior of predicting a peak in the transition temperature as a function of $|U|$, but also predicts that there is a finite value of $|U|$ below which $T_c=0$. The quantitative prediction for the peak position and peak height were much better for the Holstein model (at $\Omega=0.5$) than for the Hubbard model.

The strong-coupling approximation is also more accurate near half-filling than it is for small electron concentrations. This probably occurs because the dynamical generation of a double-well effective-phonon potential is more difficult at low electron concentrations than it is at half-filling. As a result, the fourth-order strong-coupling approximation does not predict the transition between CDW order and superconductivity accurately at $\Omega=0.5$.

The extremely good success of the fourth-order strong-coupling approximation provides a motivation for studying the conserving fluctuation-exchange approximation[30] (which is analogously the next level of weak-coupling approximations beyond the conserving Hartree-Fock approximation) to see if a unified approximation technique can carry one from the weak-coupling limit to the strong-coupling limit. Work along these lines is currently in progress.

ACKNOWLEDGMENTS

I would like to acknowledge stimulating discussions with M. Jarrell, H. Monien, R. Scalettar, and D. J. Scalapino. This research was supported by the National Science Foundation under Grants Nos. DMR90-02492 and PHY89-04035.

APPENDIX

The numerical methods used to evaluate the parameters of the effective Hamiltonian as functions of S are described here. The coefficients are expressed in the text as three-dimensional integrals that depend parametrically on S. The integrand is a strongly peaked function of x,y, and z in the large S limit so that direct numerical integration schemes are difficult to control. The three integrations can be carried out analytically, producing a power-series expansion in S for the relevant parameters. The power series involve up to fivefold iterated summations that converge quickly for values of S smaller than 5. Loss of precision occurs for some parameters when S exceeds 20. Larger values of S were not required in the numerical cases analyzed in the text.

The approach utilized for conversion of the multidimensional integrations into power series expansions is illustrated below for the coefficient α. The first step is to change variables from x,y, and z to $u=xyz$, $v=xz$, and $w=z$:

$$\alpha=-\frac{t^{*4}}{4|U|^3}S^3e^{-2S}\int_0^1\frac{dw}{w}\int_0^w\frac{dv}{v}\int_0^v du\,u^{S-1}\exp\frac{1}{2}S\left[w+\frac{v}{w}+u+\frac{u}{v}\right]. \tag{A1}$$

The integration over the variable u is performed by expanding the exponential in a power series

$$\alpha=-\frac{t^{*4}}{4|U|^3}S^2e^{-2S}\sum_{m=0}^{\infty}\frac{(S/2)^m}{m!}\frac{S}{m+S}\int_0^1\frac{dw}{w}\exp\frac{1}{2}Sw\int_0^w dv\,v^{S-1}(1+v)^m\exp\frac{1}{2}S\frac{v}{w}. \tag{A2}$$

The integration over the variable v is performed by first expanding the binomial $(1+v)^m$ with the binomial theorem, and then expanding the exponential in a power series and integrating. The result is

$$\alpha=-\frac{t^{*4}}{4|U|^3}Se^{-2S}\sum_{l,m=0}^{\infty}\sum_{n=0}^{m}\frac{(S/2)^{m+l}}{l!(m-n)!n!}\frac{S}{m+S}\frac{S}{l+n+S}\int_0^1 dw\,w^{n+S-1}\exp\frac{1}{2}Sw. \tag{A3}$$

Finally, the integration over w is performed by also expanding the exponential in a power series. The variables in the summations are then redefined in order to reexpress the power series in purely increasing powers of S. The end result is

$$\alpha=-\frac{t^{*4}}{4|U|^3}e^{-2S}\sum_{k=0}^{\infty}\left[\frac{S}{2}\right]^k\sum_{l=0}^{k}\frac{1}{(k-l)!}\sum_{m=0}^{l}\frac{1}{(l-m)!}\frac{S}{m+S}\sum_{n=0}^{m}\frac{1}{(m-n)!n!}\frac{S}{k-l+n+S}\frac{S}{l-m+n+S}. \tag{A4}$$

Similar methods are used to evaluate all of the other relevant coefficients. The final expressions are too cumbersome to be reported here.

[1]A. B. Migdal, Zh. Eksp. Teor. Fiz. **34**, 1438 (1958) [Sov. Phys. JETP **7**, 999 (1958)].
[2]G. M. Eliashberg, Zh. Eksp. Teor. Fiz. **38**, 966 (1960) [Sov. Phys. JETP **11**, 696 (1960)].
[3]S. Robaszkiewicz, R. Micnas, and K. A. Chao, Phys. Rev. B **23**, 1447 (1981); A. S. Alexandrov, J. Ranninger, and S. Robaszkiewicz, Phys. Rev. B **33**, 4526 (1986); R. Micnas, J. Ranninger, and S. Robaszkiewicz, Rev. Mod. Phys. **62**, 113 (1990).
[4]T. Holstein, Ann. Phys. (N.Y.) **8**, 325 (1959).
[5]J. Hubbard, Proc. R. Soc. London Ser. A **276**, 238 (1963); **277**, 237 (1964); **281**, 401 (1964); **285**, 542 (1965); **296**, 82 (1967); **82**, 100 (1967).
[6]C. C. Yu and P. W. Anderson, Phys. Rev. B **29**, 6165 (1984).
[7]J. Mustre de Leon, I. Bastić, A. R. Bishop, S. D. Conradson, and S. A. Trugman, Phys. Rev. Lett. **68**, 3236 (1992).
[8]A. J. Fedro and H.-B. Schüttler, Physica C **185-189**, 1673 (1991); J. Zhong and H.-B. Schüttler, Phys. Rev. Lett. **69**, 1600 (1992).
[9]J. K. Freericks, M. Jarrell, and D. J. Scalapino, Phys. Rev. B (to be published).
[10]P. W. Anderson, Phys. Rev. **115**, 2 (1959).
[11]T. Kato, Prog. Theor. Phys. **4**, 514 (1949).
[12]D. J. Klein and W. A. Seitz, Phys. Rev. B **8**, 2236 (1973).
[13]M. Takahashi, J. Phys. C **10**, 1289 (1977).
[14]G. Beni, P. Pincus, and J. Kanamori, Phys. Rev. B **10**, 1896 (1974).
[15]J. E. Hirsch and E. Fradkin, Phys. Rev. Lett. **49**, 402 (1982); Phys. Rev. B **27**, 4302 (1983).
[16]I. G. Lang and Yu. A. Firsov, Zh. Eksp. Teor. Fiz. **43**, 1843 (1962) [Sov. Phys. JETP **16**, 1301 (1963)].
[17]J. R. Schrieffer and P. A. Wolff, Phys. Rev. **149**, 491 (1966).
[18]A. B. Harris and R. V. Lange, Phys. Rev. **157**, 295 (1967).
[19]A. H. MacDonald, S. M. Girvin, and D. Yoshioka, Phys. Rev. B **37**, 9753 (1988); **41**, 2565 (1990).
[20]P. O. Löwdin, J. Chem. Phys. **18**, 365 (1950); Adv. Phys. **5**, 1 (1956).
[21]O. J. Heilmann and E. H. Lieb, Trans. N. Y. Acad. Sci. **33**, 116 (1971); C. N. Yang, Phys. Rev. Lett. **63**, 2144 (1989); M. Pernici, Europhys. Lett. **12**, 75 (1989); S. Zhang, Phys. Rev. Lett. **65**, 120 (1990).
[22]The pseudospin operators have the phase $(-1)^j$ introduced on bipartite lattices so that the total pseudospin operator will commute with the Holstein Hamiltonian in the Hubbard model limit ($\Omega \rightarrow \infty$). If the lattice is not bipartite, the mapping can be made to pseudospin operators without the additional phase factor. The only differences will be to change the sign of the parameters $j_\perp^{(2)}$ in H_2, $j_\perp^{(4)}$ in $H_4(b)$, $j_\perp'$ in $H_4(c)$, and β and ϵ in $H_4(d)$. The superconducting transition temperature will be the temperature where $\langle J^x \rangle = m'/2$ and $\langle J^z \rangle = m/2$ in the limit $m' \rightarrow 0$.
[23]W. Metzner and D. Vollhardt, Phys. Rev. Lett. **62**, 324 (1989).
[24]C. J. Gorter, Rev. Mod. Phys. **25**, 277 (1953).
[25]M. Jarrell, Phys. Rev. Lett. **69**, 168 (1992).
[26]M. Jarrell and T. Pruschke, Z. Phys. B **90**, 187 (1993).
[27]A. Georges and W. Krauth, Phys. Rev. Lett. **69**, 1240 (1992); (unpublished).
[28]R. T. Scalettar, D. J. Scalapino, R. L. Sugar, and D. Toussaint, Phys. Rev. B **39**, 4711 (1989).
[29]The transition temperature at half-filling is independent of the sign of U. The quantum Monte Carlo algorithm for positive U begins to fail at $U \approx 4$. The algorithm remains stable for negative U up to $|U| \approx 6$. The data in Fig. 2 are the positive U results of Jarrell (Ref. 25) for $|U| \leq 3.5$; the data points at $U = -4$, -4.5, and -6 were calculated using a negative U algorithm. Both the negative and positive U algorithms agree to within 0.4% at $|U| = 3$.
[30]N. E. Bickers and D. J. Scalapino, Ann. Phys. (N.Y.) **193**, 206 (1989).